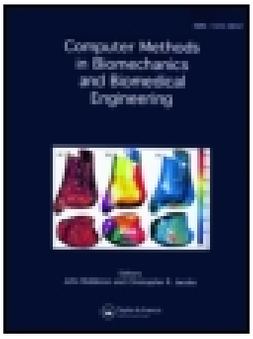

Computer Methods in Biomechanics and Biomedical Engineering

ISSN: (Print) (Online) Journal homepage: https://www.tandfonline.com/loi/gcmb20

Tibiofemoral forces during FES rowing in individuals with spinal cord injury

Vishnu D. Chandran , Rebecca L. Lambach , Robin S. Gibbons , Brian J. Andrews , Gary S. Beaupre & Saikat Pal

To cite this article: Vishnu D. Chandran , Rebecca L. Lambach , Robin S. Gibbons , Brian J. Andrews , Gary S. Beaupre & Saikat Pal (2020): Tibiofemoral forces during FES rowing in individuals with spinal cord injury, Computer Methods in Biomechanics and Biomedical Engineering, DOI: 10.1080/10255842.2020.1821880

To link to this article: https://doi.org/10.1080/10255842.2020.1821880

Published online: 17 Sep 2020.

Submit your article to this journal

View related articles

View Crossmark data

Full Terms & Conditions of access and use can be found at
https://www.tandfonline.com/action/journalInformation?journalCode=gcmb20

COMPUTER METHODS IN BIOMECHANICS AND BIOMEDICAL ENGINEERING
https://doi.org/10.1080/10255842.2020.1821880

Taylor & Francis
Taylor & Francis Group

Check for updates

Tibiofemoral forces during FES rowing in individuals with spinal cord injury

Vishnu D. Chandran[a], Rebecca L. Lambach[b], Robin S. Gibbons[c], Brian J. Andrews[d,e], Gary S. Beaupre[b] and Saikat Pal[a,f]

[a]Department of Biomedical Engineering, New Jersey Institute of Technology, Newark, NJ, USA; [b]Musculoskeletal Research Laboratory, VA Palo Alto Health Care System, Palo Alto, CA, USA; [c]Centre for Rehabilitation Engineering and Assistive Technologies, University College London, Stanmore, UK; [d]Nuffield Department of Surgical Sciences, University of Oxford, Oxford, UK; [e]Biomedical Engineering Group, School of Engineering, Warwick University, Coventry, UK; [f]Department of Electrical and Computer Engineering, New Jersey Institute of Technology, Newark, NJ, USA

ABSTRACT

The purpose of this study is to determine the tibiofemoral forces during functional electrical stimulation (FES) rowing in individuals with spinal cord injury (SCI). We analysed the motion of five participants with SCI during FES rowing, with simultaneous measurements of (i) three-dimensional marker trajectories, (ii) foot reaction forces (FRFs), (iii) ergometer handle forces, and (iv) timestamps for electrical stimulation of the quadriceps and hamstrings muscles. We created full-body musculoskeletal models in OpenSim to determine subject-specific tibiofemoral forces during FES rowing. The peak magnitudes of tibiofemoral forces averaged over five participants with SCI were 2.43 ± 0.39 BW and 2.25 ± 0.71 BW for the left and right legs, respectively. The peak magnitudes of FRFs were 0.19 ± 0.04 BW in each leg. The peak magnitude of handle forces was 0.47 ± 0.19 BW. Peak tibiofemoral force was associated with peak FRF (magnitudes, $R^2 = 0.56$, $p = 0.013$) and peak handle force (magnitudes, $R^2 = 0.54$, $p = 0.016$). The ratios of peak magnitude of tibiofemoral force to peak magnitude of FRF were 12.9 ± 1.9 (left) and 11.6 ± 2.4 (right), and to peak magnitude of handle force were 5.7 ± 2.3 (left) and 4.9 ± 0.9 (right). This work lays the foundation for developing a direct exercise intensity metric for bone mechanical stimulus at the knee during rehabilitation exercises. Clinical Significance: Knowledge of tibiofemoral forces from exercises such as FES rowing may provide clinicians the ability to personalize rehabilitation protocols to ensure that an SCI patient is receiving the minimum dose of mechanical stimulus necessary to maintain bone health.

ARTICLE HISTORY
Received 24 June 2020
Accepted 7 September 2020

KEYWORDS
Tibiofemoral force; FES rowing; spinal cord injury; musculoskeletal modelling; functional electrical stimulation

Introduction

Immobilization osteoporosis is a well-known secondary complication of spinal cord injury (SCI), with up to 73% bone at the epiphyses resorbed within the first few years after injury (Eser et al. 2004, 2005). These losses are likely superimposed on continual age-related bone loss (Bauman and Cardozo 2015). Spinal cord injury-related weakened bones are at high risk of fragility fractures, with an estimated 70%–76% of individuals with SCI sustaining a low-impact or pathologic fracture during their lifetime (Szollar et al. 1998; Morse et al. 2009b). Over 80% of fragility fractures occur in the lower extremities, with the most common fracture site being the knee region (distal femur and proximal tibia) (Grassner et al. 2018). These fractures often result in complications, prolonged hospitalization, and patient morbidity (Morse et al. 2009a) and mortality (Krause et al. 2008).

Mechanical stimulation of bone through exercise is the primary mechanism of non-pharmacologic therapy for bone loss after SCI, consistent with the able-bodied population (Beck and Snow 2003; Martelli et al. 2020). Bone loss after SCI is largely a function of disuse, due to the absence of forces from voluntary muscle contraction and the inability to perform weight-bearing activities. Different rehabilitation exercises have been used to induce muscle forces and reproduce weight-bearing activities for mechanical stimulation of bone after SCI, including weight-bearing standing (Ben et al. 2005; Alekna et al. 2008), body weight-supported treadmill training (Giangregorio et al. 2005), standing wheelchair (Goemaere et al. 1994), functional electrical stimulation (FES) of specific muscles groups (Shields and Dudley-Javoroski 2007), and FES knee extension (Clark et al. 2007). FES cycling is another exercise clinically available for promoting bone health after SCI (Bloomfield et al. 1996; Mohr et al. 1997; Johnston et al.

CONTACT Saikat Pal pal@njit.edu
© 2020 Informa UK Limited, trading as Taylor & Francis Group

Table 1. Participant and FES rowing characteristics.

Subject	Age (years)	Sex	Mass (kg)	Height (cm)	Time post-SCI (months)	Injury level	AISA Scale	Rail angle (°)	Rowing stroke interval (s)
1	43	Male	86.9	175	16	T4	A	5.6	2.4
2	35	Male	96.3	191	11	T10	A	3.9	2.2
3	29	Male	107.9	188	13	T2	B	5.7	2.1
4	34	Male	87.3	188	7	T5	A	3.3	2.0
5	23	Male	61.3	191	10	C7	B	4.8	1.7

AISA Scale: American Spinal Injury Association Impairment Scale. A score of A corresponds to complete impairment, sensory and motor, below the neurological level; B corresponds to some sensory but no motor function below the neurological level.

2016). The repetitive motion from FES cycling has been shown to be beneficial for a range of health measures (Dolbow et al. 2013; Fornusek et al. 2013; Gorgey and Lawrence 2016; Johnston et al. 2016); these benefits explain the widespread acceptance of FES cycling within the SCI community.

Despite the prevalence of different rehabilitation exercises for mechanical stimulation of bone after SCI, the efficacy of these exercises to prevent, reverse, or even modulate bone loss has been vastly inconsistent to date. Using FES cycling interventions, some studies targeting bone loss at the knee joint have reported significant increases in bone densities (Chen et al. 2005; Frotzler et al. 2008; Gibbons et al. 2016), while other studies have reported no such improvements (Pacy et al. 1988; Johnston et al. 2016). An intuitive explanation for these inconsistencies in the literature is varying levels of exercise intensity among studies. Indeed, the studies that reported increases in bone densities following FES cycling interventions reported substantially greater exercise intensities (Chen et al. 2005; Frotzler et al. 2008; Gibbons et al. 2016) compared to studies with no improvements in bone densities (Pacy et al. 1988; Johnston et al. 2016). Since early reports from 1990s (Andrews et al. 2017), FES rowing has grown in popularity as an alternative to FES cycling largely because rowing is associated with higher exercise intensity at the knee compared to cycling; cycling is considered a non-weight bearing exercise (Nichols et al. 2003). In rowing, a relatively large mass (torso) is accelerated from rest at low cadence, whereas in cycling, low masses (feet) are moving at relatively constant velocity at low cadence. Early indications from small cohort studies of FES rowing interventions are promising in regards to bone mineral density (Gibbons et al. 2014, 2016; Deley et al. 2017; Lambach et al. 2020) and bone microstructure (Draghici et al. 2019), highlighting the importance of exercise intensity for mitigating bone loss after SCI.

Although there is compelling evidence that exercise intensity is a key factor for mitigating bone loss after SCI, no uniformly accepted definition of exercise intensity exists in the literature. Previous studies have reported exercise intensity using machine resistance (Dolbow et al. 2017), work load (Pacy et al. 1988; Mohr et al. 1997), power output (Bloomfield et al. 1996; Frotzler et al. 2008; Griffin et al. 2009; Johnston et al. 2016), pedal revolutions per session (Bloomfield et al. 1996), work (Mohr et al. 1997; Griffin et al. 2009), and torque (Johnston et al. 2016). There is no consensus on an exercise intensity metric, which adds to the confusion in the literature. Further, these exercise machine-based metrics are a surrogate measure for mechanical stimulus within the bone. Currently, there is no direct metric for bone mechanical stimulus during exercise because quantifying bone mechanical stimulus, for example at the knee, requires knowledge of tibiofemoral forces. Quantifying tibiofemoral forces during dynamic activities is difficult. Experimental methods are too invasive and currently infeasible; the only feasible option is using computational simulation. Accordingly, the goal of this study was to determine the tibiofemoral forces during FES rowing in individuals with SCI using a combination of motion capture experiments and computational simulations. Specifically, we addressed the following research questions: (1) What are the peak tibiofemoral forces during FES rowing in individuals with SCI? (2) What are the peak foot reaction and handle forces during FES rowing in individuals with SCI? (3) Are there relationships between peak tibiofemoral force and peak foot reaction force (FRF), and peak handle force, during FES rowing in individuals with SCI? (4) What are the ratios of peak tibiofemoral forces to peak FRFs and handle forces during FES rowing in individuals with SCI? (5) What are the patterns in tibiofemoral, foot reaction, and handle forces among SCI subjects during FES rowing? We hypothesized that computed tibiofemoral forces will be larger than measured FRFs and handle forces and sought to quantify these relationships.

Materials and methods

Participant recruitment

We recruited five participants with acute, traumatic, motor complete SCI, C7-T12, American Spinal Injury Association Impairment Scale A or B, who were

3–24 months post-injury (Table 1) (Lambach et al. 2020). The inclusion criteria were 18-years or older; a physician's clearance to exercise; adequate passive hip, knee, and ankle range of motion to perform rowing; ability to perform safe, independent transfers; and responsiveness to muscle stimulation of the quadriceps and hamstrings without significant or uncontrolled symptoms of autonomic dysreflexia. Exclusion criteria were pregnancy, lower limb fracture since SCI, additional medical conditions that impact bone metabolism (e.g. renal disease), use of medications affecting bone density (e.g. bisphosphonates), additional neurological diseases, implanted electronic devices (e.g. pacemaker), current thrombosis, active pressure sores, coronary artery disease, and family history of sudden cardiac death. Prior to participation, each participant was informed on all aspects of the study and provided signed consent according to the policies of an Institutional Review Board.

Muscle conditioning and FES rowing exercise intervention

All participants underwent a muscle conditioning program, followed by an FES rowing intervention (Lambach et al. 2020). The participants completed the muscle conditioning program to develop sufficient strength and endurance in the quadriceps and hamstrings muscles. The conditioning program consisted of seated FES leg extension/flexion. The criterion for progressing from muscle conditioning to FES rowing was a participant's ability to perform FES conditioning continuously for 30 minutes, maintaining full knee extension throughout the duration of a session. The muscle conditioning program varied from two to eight weeks for all five participants. The FES rowing intervention comprised 90 sessions over a 9- to 12-month period, with up to 30 minutes of active rowing time per session. We used a modified Concept2 Model D ergometer (Concept2, Morrisville, VT) with adapted components (Paddlesport, East Hardwick, VT) to provide trunk stability and prevent lateral leg movement in participants with SCI (Figure 1(A)). A modified frame monorail was attached to accommodate a larger seat and to allow for inclination of the monorail for gravity-assistance during the recovery (active leg flexion) phase of the rowing motion while increasing lower limb forces during the drive (active leg extension) phase. Prior to an FES rowing session, the rail angle was set at the highest possible value that a participant could complete a full stroke (Table 1). We used a four-channel electrical stimulator (Odstock

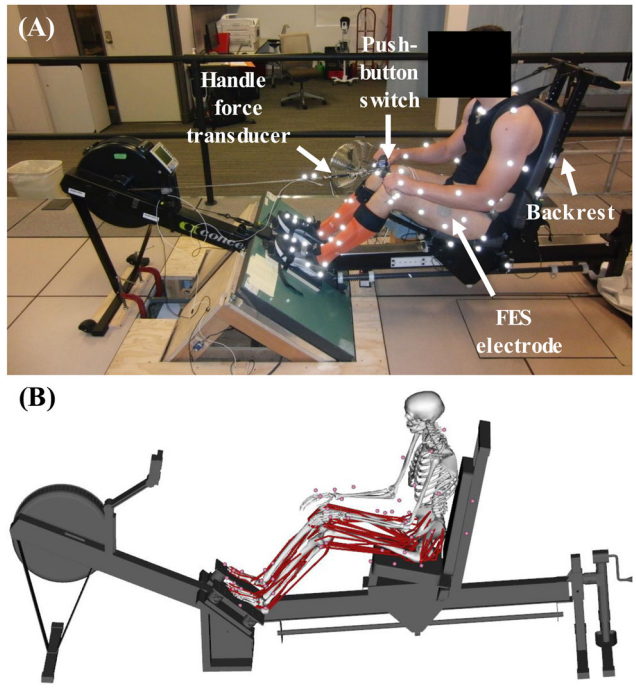

Figure 1. A representative participant with SCI during (A) FES rowing, and the corresponding musculoskeletal model to determine subject-specific tibiofemoral forces (B). A Concept 2 Model D ergometer was modified to include a backrest for trunk stability, and foot stretchers were replaced with angle-mounted force plates to measure foot reaction forces. The handle was instrumented with an inline force transducer to measure forces during rowing.

O4CHS; Odstock Medical Ltd., Salisbury, UK) with self-adhesive 2.75 inch diameter round surface electrodes (Pals Platinum; Axelgaard Manufacturing Company Ltd, Fallbrook, CA) to deliver bilateral stimulation to the quadriceps and hamstrings muscles. Electrode placement was based on determining the motor points, which differ between individuals and legs. For the quadriceps muscles, the indifferent electrode was placed anterior-medially above the knee, while the active electrode was placed anterior-laterally at approximately the mid-thigh level. For the hamstrings muscles, the indifferent electrode was placed posterior-centrally above the knee, while the active electrode was placed posterior-centrally over the center of the muscle belly, approximately 5 cm above the indifferent electrode. The electrode locations were checked often and moved, if necessary, to obtain the best possible muscle stimulation. The FES parameters were: pulse width 450 μs and pulse frequency 40 Hz. Current amplitude varied between 0–120 mA; the amplitude was adjusted throughout each session for the quadriceps to produce full knee extension and for the hamstrings to produce visible knee flexion. A participant controlled the stimulation timing manually

using a push-button switch attached to the ergometer handle; pushing the button activated the quadriceps and releasing the button activated the hamstrings. We trained the participants to row using a technique that follows that of able-bodied rowing, with leg extension synchronized with arm pull during the drive phase (video available as supplemental material in Lambach et al. 2020). Participants were instructed to keep their arms fully extended during early leg extension and to flex their arms as the legs reached mid- to near-full extension. The early FES rowing sessions comprised short intervals (1–3 minutes) and progressed until participants could perform 30 minutes of continuous FES rowing with occasional short hydration breaks.

Motion capture experiments during FES rowing

We analysed the motion of each participant during FES rowing, with simultaneous measurements of three-dimensional marker trajectories, foot reaction forces, ergometer handle forces, and timestamps for electrical stimulation of the quadriceps and hamstrings muscles (Figure 1(A)). A 10-camera motion capture system (Qualisys, Goteburg, Sweden) was used to analyse full-body motion. Marker trajectories during FES rowing were sampled at 120 Hz. We recorded reaction forces from each foot during FES rowing using two force plates (Bertec Corp., Columbus, OH). We modified the ergometer and mounted the force plates to replicate the angle and position of the ergometer foot-stretchers (Figure 1(A)). The force plates were mounted on custom support structures that were bolted to the concrete floor. The original foot-stretchers were removed from the ergometer, and foot-stretcher covers were affixed to the surface of the two force plates. The participant's feet were strapped directly to the force plates during FES rowing. We recorded ergometer handle forces using an inline force sensor (model ELHS, Measurement Specialties, Aliso Viejo, CA) attached to the handle cable. The force data were filtered using a low-pass, fourth-order Butterworth filter with a cutoff frequency of 10–25 Hz. We recorded the timestamps corresponding to the activation and release of the push-button switch, denoting stimulation of the quadriceps and hamstrings, respectively. The sampling frequency for the force plates, handle sensor, and push-button switch was 960 Hz. Prior to data collection, participants warmed up for approximately five minutes, after which data were recorded for 20 seconds during continuous FES rowing. Motion capture data from five consecutive rowing strokes, beginning and ending with a participant at the catch or forward-most position, was selected for further analysis. This motion capture data collection was performed at weeks 12, 24, and 36 of the FES rowing intervention.

Musculoskeletal modelling

We created full-body musculoskeletal models in OpenSim (Delp et al. 2007) to compute subject-specific tibiofemoral forces during FES rowing (Figure 1(B)). For this study, we used the motion capture data from week 36 for all participants. We integrated a previously-published musculoskeletal model (Rajagopal et al. 2016) with a full-scale geometry of the SCI-adapted ergometer. The integrated full-body and ergometer model had 24 segments and 32 degrees of freedom (DoFs): seven in each leg, three at the torso, seven in each arm, and one between the seat and the ergometer rail. The seven DoFs in each leg included three DoFs at the ball-and-socket hip joint, a one DoF coupled knee mechanism with translations of the tibia and patella prescribed by the knee flexion angle, and one DoF revolute joints at the ankle, subtalar, and metatarsal joints. The three DoFs in the torso and upper body included a spherical joint connecting the torso to the pelvis. The seven DoFs in each arm included three DoFs at the ball-and-socket shoulder joint, one DoF revolute joint at the elbow, one DoF revolute joint between the radius and the ulna, and two DoFs universal joint between the radius and the hand for wrist flexion-extension and radial-ulnar deviation. In addition, there was a single degree of freedom slider joint connecting the seat to the ergometer rail. The model's pelvis was welded to the ergometer seat, and the position and orientation of the pelvis with respect to the seat were derived from the marker trajectories. The model's feet were constrained to the footrests using a custom point (rotational only) constraint in OpenSim. The model was driven by 80 Hill-type muscle-tendon actuators (Thelen et al. 2003) that generated moments to reproduce motion at the lower extremities, and 18 ideal torque actuators to displace the torso and the upper body. The Hill-type muscle-tendon actuators captured the force-length-velocity properties of the lower extremity muscles, with muscle geometry and architecture based on adult cadaver data (Delp et al. 1990).

We adapted a previously published computational framework in OpenSim to determine subject-specific tibiofemoral forces during FES rowing (Delp et al. 2007; Rajagopal et al. 2016). We scaled the generic musculoskeletal model to match the mass and segment lengths of each participant with SCI; this

ensured that all joint kinematics, muscle attachments, and muscle moment arms were scaled to the anthropometry of each participant. We adjusted the optimal fiber length and tendon slack length of each of the lower extremity muscles using a manual process to ensure the muscles produced active and passive forces at the desired joint angles. Other muscle parameters, including pennation angles and maximum isometric forces, were not altered. We determined joint kinematics by performing Inverse Kinematics (IK) analysis in OpenSim. IK solves for kinematics by minimizing error between the experimentally measured marker positions and the corresponding markers on the musculoskeletal model. We performed inverse dynamics analyses to compute subject-specific net joint torques. Next, we performed forward dynamics analyses, comprising Residual Reduction Algorithm (RRA) and Computed Muscle Control (CMC), to determine subject-specific muscle forces during FES rowing (Delp et al. 2007). Residual Reduction Algorithm checks for dynamic consistency of the forces in the model and provides adjusted kinematics the model can track with ideal torque actuators (Delp et al. 2007). We performed IK, inverse dynamics, and RRA on all five consecutive strokes of FES rowing; we performed CMC on the first complete stroke of FES rowing from each participant. CMC computes muscle excitation to match the adjusted joint kinematics (Thelen et al. 2003). To simulate FES-controlled muscle activation, CMC computed the muscle excitations in the quadriceps and hamstrings muscles corresponding to when they were stimulated during the stroke cycle. The excitation levels of all other muscles were set to zero to simulate no active recruitment of muscles in motor-complete SCI patients; the model permitted passive forces in all muscles. Computed Muscle Control was able to match the joint kinematics well in all five subject-specific models, with an average difference between experimentally-derived and CMC-predicted joint kinematics being less than 2.6° in all cases. Finally, we computed the tibiofemoral forces during FES rowing using the Joint Reaction Analysis module in OpenSim, which summed the contributions of the muscle forces and reaction loads at the knee joint (Steele et al. 2012; DeMers et al. 2014).

Data analysis and statistical methods

We determined peak tibiofemoral forces and FRFs in each leg during FES rowing from all five participants. The peak magnitudes and corresponding peak compressive, AP shear, and ML shear components of the tibiofemoral forces and FRFs from each participant were averaged for each leg over all five participants. The peak magnitudes of handle forces from each participant were averaged over all five participants. All forces were normalized to each participant's body weight. Next, we evaluated the relationships between peak tibiofemoral forces and peak FRFs, and peak handle forces. Linear regression models were used to test for the significance of a relationship ($p < 0.050$). Finally, we determined the ratios of peak tibiofemoral forces to peak FRFs, and peak handle forces from all five participants. The ratios of peak tibiofemoral forces to peak FRFs were obtained for the peak magnitudes and corresponding peak compressive, AP shear, and ML shear components from each participant and averaged for each leg over all five participants. The ratios of peak tibiofemoral forces to peak handle forces were obtained for the peak magnitude, compressive, AP shear, and ML shear components of tibiofemoral forces to peak magnitude of handle force from each participant and averaged for each leg over all five participants.

Results

The peak magnitude of tibiofemoral forces during FES rowing averaged over five participants with SCI were 2.43 ± 0.39 BW (left) and 2.25 ± 0.71 BW (right), ranging from 1.97–2.97 BW and 1.25–3.25 BW for the left and right legs, respectively (Figure 2). The peak compressive tibiofemoral forces were 2.36 ± 0.37 BW (left) and 2.19 ± 0.70 BW (right), ranging from 1.93–2.88 BW and 1.21–3.17 BW for the left and right legs, respectively. The peak AP shear tibiofemoral forces were 0.42 ± 0.09 BW (left) and 0.36 ± 0.15 BW (right), ranging from 0.32–0.52 BW and 0.21–0.58 BW for the left and right legs, respectively. The peak ML shear tibiofemoral forces were 0.83 ± 0.29 BW (left) and 0.46 ± 0.18 BW (right), ranging from 0.52–1.19 BW and 0.23–0.72 BW for the left and right legs, respectively.

The peak magnitudes of FRFs during FES rowing averaged over five participants with SCI were 0.19 ± 0.04 BW in each leg, ranging from 0.15–0.26 BW and 0.17–0.26 BW for the left and right legs, respectively (Figure 3). The peak compressive FRFs were 0.14 ± 0.02 BW (left) and 0.13 ± 0.03 BW (right), ranging from 0.12–0.16 BW and 0.11–0.17 BW for the left and right legs, respectively. The peak AP shear FRFs were 0.14 ± 0.04 BW (left) and 0.14 ± 0.03 BW (right), ranging from 0.11–0.20 BW and 0.12–0.19 BW for the left and right legs, respectively. The peak

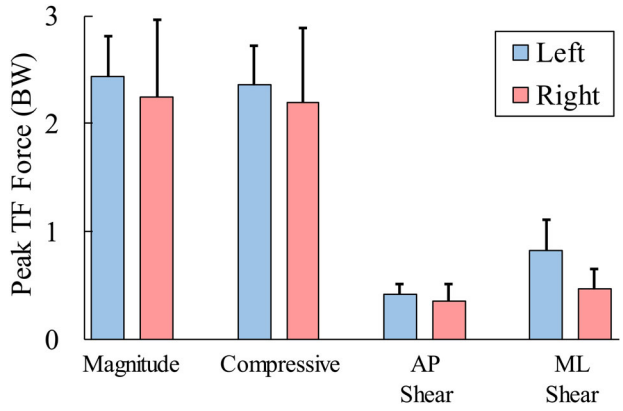

Figure 2. Peak tibiofemoral (TF) forces during FES rowing in individuals with SCI. The peak magnitudes and corresponding peak compressive, anterior-posterior (AP) shear, and medial-lateral (ML) shear components of TF forces from each participant were averaged for each leg over all five participants. All forces were normalized to each participant's body weight (BW). The error bars represent +1 SD.

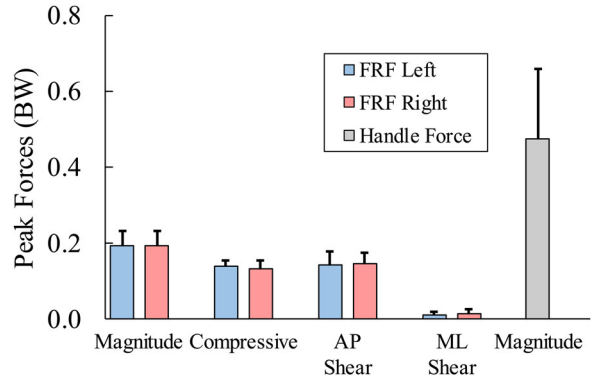

Figure 3. Peak foot reaction forces (FRF) and peak handle forces during FES rowing in individuals with SCI. The peak magnitudes and corresponding peak compressive, anterior-posterior (AP) shear, and medial-lateral (ML) shear components of FRFs from each participant were averaged for each leg over all five participants. The peak magnitudes of handle forces from each participant were averaged over all five participants. All forces were normalized to each participant's body weight (BW). The error bars represent +1 SD.

ML shear FRFs were 0.010 ± 0.006 BW (left) and 0.014 ± 0.011 BW (right), ranging from 0.004–0.017 BW and 0.001–0.029 BW for the left and right legs, respectively. The peak magnitude of handle forces during FES rowing averaged over five participants with SCI was 0.47 ± 0.19 BW, ranging from 0.25–0.68 BW (Figure 3).

Peak tibiofemoral force was associated with peak FRF (magnitudes, $R^2 = 0.56$, $p = 0.013$) and peak handle force (magnitudes, $R^2 = 0.54$, $p = 0.016$) (Figure 4(A,C)). Resolving the magnitudes of forces into their components, we found a significant relationship between the peak compressive components of tibiofemoral force and FRF ($R^2 = 0.54$, $p = 0.016$); we found no relationship between the peak AP and ML shear components of tibiofemoral force and FRF (Figure 4(B)). We found a significant relationship between the peak compressive component of tibiofemoral force and peak magnitude of handle force ($R^2 = 0.51$, $p = 0.020$); we found no relationship between the peak AP and ML shear components of tibiofemoral force and peak magnitude of handle force (Figure 4(D)).

The ratios of peak magnitude of tibiofemoral force to peak magnitude of FRF averaged over five participants with SCI were 12.9 ± 1.9 (left) and 11.6 ± 2.4 (right) (Figure 5(A)). The ratios of peak compressive tibiofemoral force to peak compressive FRF were 17.3 ± 2.0 (left) and 16.9 ± 4.0 (right). The ratios of peak AP shear tibiofemoral force to peak AP shear FRF were 3.0 ± 0.8 (left) and 2.4 ± 0.8 (right). The ratios of peak magnitude of tibiofemoral force to peak magnitude of handle force averaged over five participants with SCI were 5.7 ± 2.3 (left) and 4.9 ± 0.9 (right) (Figure 5(B)). The ratios of peak compressive tibiofemoral force to peak magnitude of handle force were 5.6 ± 2.3 (left) and 4.8 ± 1.0 (right). The ratios of peak AP shear tibiofemoral force to peak magnitude of handle force were 1.0 ± 0.5 (left) and 0.8 ± 0.2 (right). The ratios of peak ML shear tibiofemoral force to peak magnitude of handle force were 1.9 ± 0.9 (left) and 1.0 ± 0.1 (right).

Tibiofemoral and FRF patterns varied among participants, while handle force patterns were consistent between participants (Figure 6). Peak tibiofemoral forces were observed during the drive phase in four out of five participants; however, in Subject 2, peak tibiofemoral force occurred during the recovery phase. These variations in tibiofemoral forces were consistent with the variations in measured FRFs; in Subject 2, the temporal locations of the computed peak tibiofemoral force and measured peak FRF were identical. In contrast, the temporal locations of peak handle forces were consistently close to the transition from drive to recovery phase. The initiation of quadriceps stimulation varied among participants; Subjects 1 and 2 activated their quadriceps at the onset of the drive phase, while Subjects 3, 4, and 5 activated their quadriceps prior to the onset of the drive phase (Figure 6).

Joint kinematics and moments varied substantially between participants, with results from a representative participant shown here (Figure 7). The CMC-predicted muscle activations were present only when electrical stimulation was present (Figure 7). The RMS errors between CMC-predicted and inverse

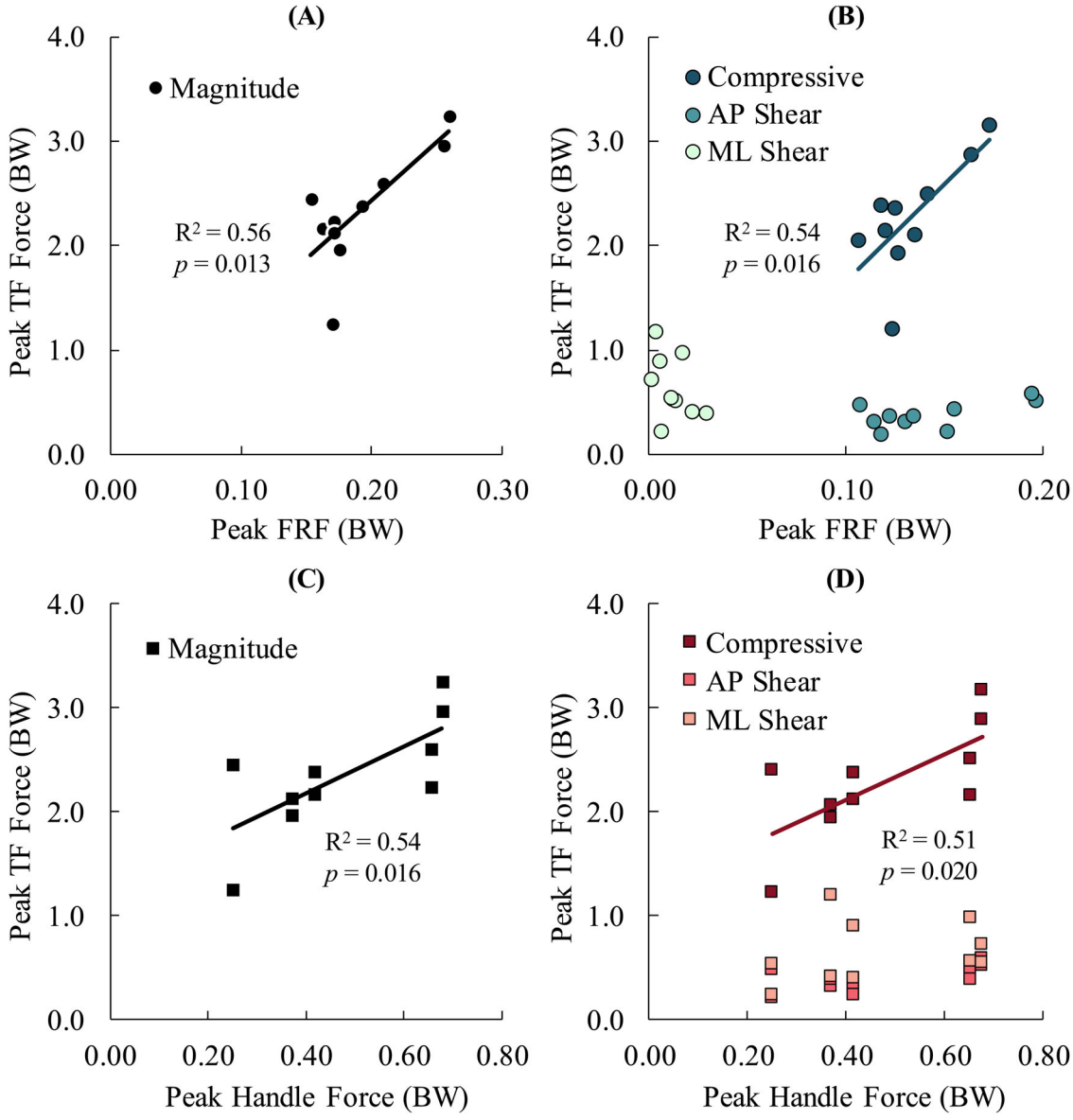

Figure 4. Relationships between peak tibiofemoral (TF) forces and (A, B) peak foot reaction forces (FRF), and (C, D) peak handle forces, during FES rowing in individuals with SCI. The relationships between TF and FRFs were quantified for (A) peak magnitudes of forces and (B) their corresponding peak compressive, anterior-posterior (AP) shear, and medial-lateral (ML) shear components. The relationships between TF forces and handle forces were quantified for the (C) peak magnitudes and (D) peak compressive, AP shear, and ML shear components of TF force to peak magnitudes of handle forces. The regression lines represent significant relationships between peak magnitudes of TF forces and FRFs ($R^2 = 0.56$, $p = 0.013$), and handle forces ($R^2 = 0.54$, $p = 0.016$); and between peak compressive TF forces and FRFs ($R^2 = 0.54$, $p = 0.016$), and peak magnitudes of handle forces ($R^2 = 0.51$, $p = 0.020$). All forces were normalized to each participant's body weight (BW).

dynamics-based knee joint moments ranged from 4.8 N·m to 16.0 N·m from all five participants (Figure 8).

Discussion

The purpose of this study was to determine the tibiofemoral forces during FES rowing in individuals with SCI. We sought to answer five research questions. Our first research question was: what are the peak tibiofemoral forces during FES rowing in individuals with SCI? The peak magnitudes of tibiofemoral forces were 2.43 ± 0.39 BW and 2.25 ± 0.71 BW for the left and right legs, respectively (Figure 2). Our second research question was: what are the peak FRFs and handle forces during FES rowing in individuals with SCI? The peak magnitudes of FRFs were 0.19 ± 0.04 BW in each leg (Figure 3). The peak magnitude of handle forces was 0.47 ± 0.19 BW during FES rowing (Figure 3). Our third research question was: are there

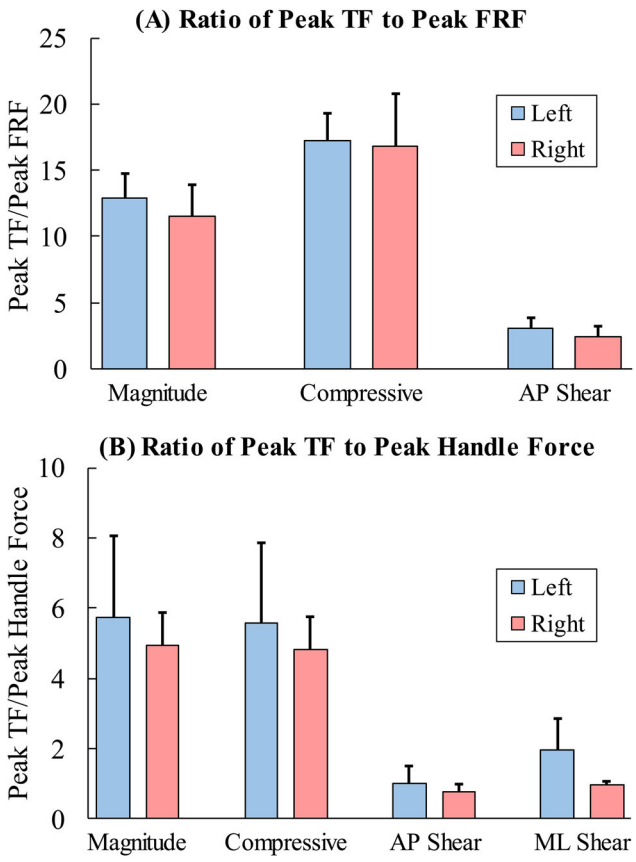

Figure 5. Average (+1 SD) ratios of peak tibiofemoral (TF) forces to (A) peak foot reaction forces (FRFs), and (B) peak handle forces, during FES rowing in individuals with SCI. The ratios of peak TF forces to peak FRFs were obtained for the peak magnitudes and corresponding peak compressive, anterior-posterior (AP) shear, and medial-lateral (ML) shear components from each participant and averaged for each leg over all five participants (A). The ratios of peak TF forces to peak handle forces were obtained for the peak magnitude, compressive, AP shear, and ML shear components of TF forces to peak magnitude of handle force from each participant and averaged for each leg over all five participants (B). The error bars represent +1 SD. The ratios for peak ML TF force to peak ML FRFs are not shown in (A) because of the negligible ML FRFs generated during FES rowing.

relationships between peak tibiofemoral force and peak FRF, and peak handle force, during FES rowing in individuals with SCI? Our results showed associations between peak tibiofemoral force and peak FRF, and peak handle force, in the magnitudes and their corresponding compressive components (Figure 4). Our fourth research question was: what are the ratios of peak tibiofemoral forces to peak FRFs and handle forces during FES rowing in individuals with SCI? The ratios of peak magnitude of tibiofemoral force to peak magnitude of FRF were 12.9 ± 1.9 and 11.6 ± 2.4 for the left and right legs, respectively (Figure 5(A)). The ratios of peak magnitude of tibiofemoral force to peak magnitude of handle force were 5.7 ± 2.3 and 4.9 ± 0.9 for the left and right legs, respectively (Figure 5(B)). Our final research question was: what are the patterns in tibiofemoral, foot reaction, and handle forces among SCI subjects during FES rowing? We found that tibiofemoral and FRF patterns varied among participants, while handle force patterns were consistent between participants (Figure 6).

Our study quantifies tibiofemoral forces during FES rowing from a cohort of participants with SCI. A prior case study reported tibiofemoral forces during FES rowing from a single participant with SCI using an inverse dynamics software package (Biomechanics of Body, Coventry University, Coventry, UK) (Gibbons et al. 2014). That case study reported peak magnitudes of tibiofemoral forces of 4.60 ± 0.40 BW in the left leg and 4.00 ± 0.80 BW in the right leg (Gibbons et al. 2014; Gibbons 2015). Those forces are substantially higher than our findings of 2.43 ± 0.39 BW (range: 1.97–2.97 BW) and 2.25 ± 0.71 BW (range: 1.25–3.25 BW) in the left and right legs, respectively (Figure 2). A possible explanation for these differences is the experience level of the rowers in the two studies. Our study included five participants who were relatively inexperienced FES rowers, and within two years of injury (Table 1). In contrast, the prior case study included a participant with >8 years of experience in FES rowing and 13.5 years post-injury (Gibbons et al. 2014; Gibbons 2015). It is plausible that training results in greater tibiofemoral forces during FES rowing. Next, our measured FRFs and handle forces were consistent with previous studies of FES rowing in individuals with SCI (Halliday et al. 2004; Gibbons et al. 2014; Gibbons 2015; Draghici et al. 2019). Halliday et al. reported peak FRFs of 0.25 BW (compressive), 0.34 BW (AP shear), and 0.11 BW (ML shear), and peak handle force of 0.40 BW from a single participant with SCI during FES rowing (Halliday et al. 2004); these forces are comparable to peak FRF and handle forces reported in this study (Figure 3).

Our results demonstrating significant associations between peak tibiofemoral forces and peak FRFs (Figure 4(A,B)) during FES rowing may have important implications in developing an evidence-based exercise intensity metric for widespread use in rehabilitation clinics and in-home therapy. Determining tibiofemoral forces require sophisticated computational modelling, which is difficult to perform outside research settings. However, once adequate regression equations are established, FRFs may be obtained using inexpensive force plates mounted on to exercise machines and may provide a

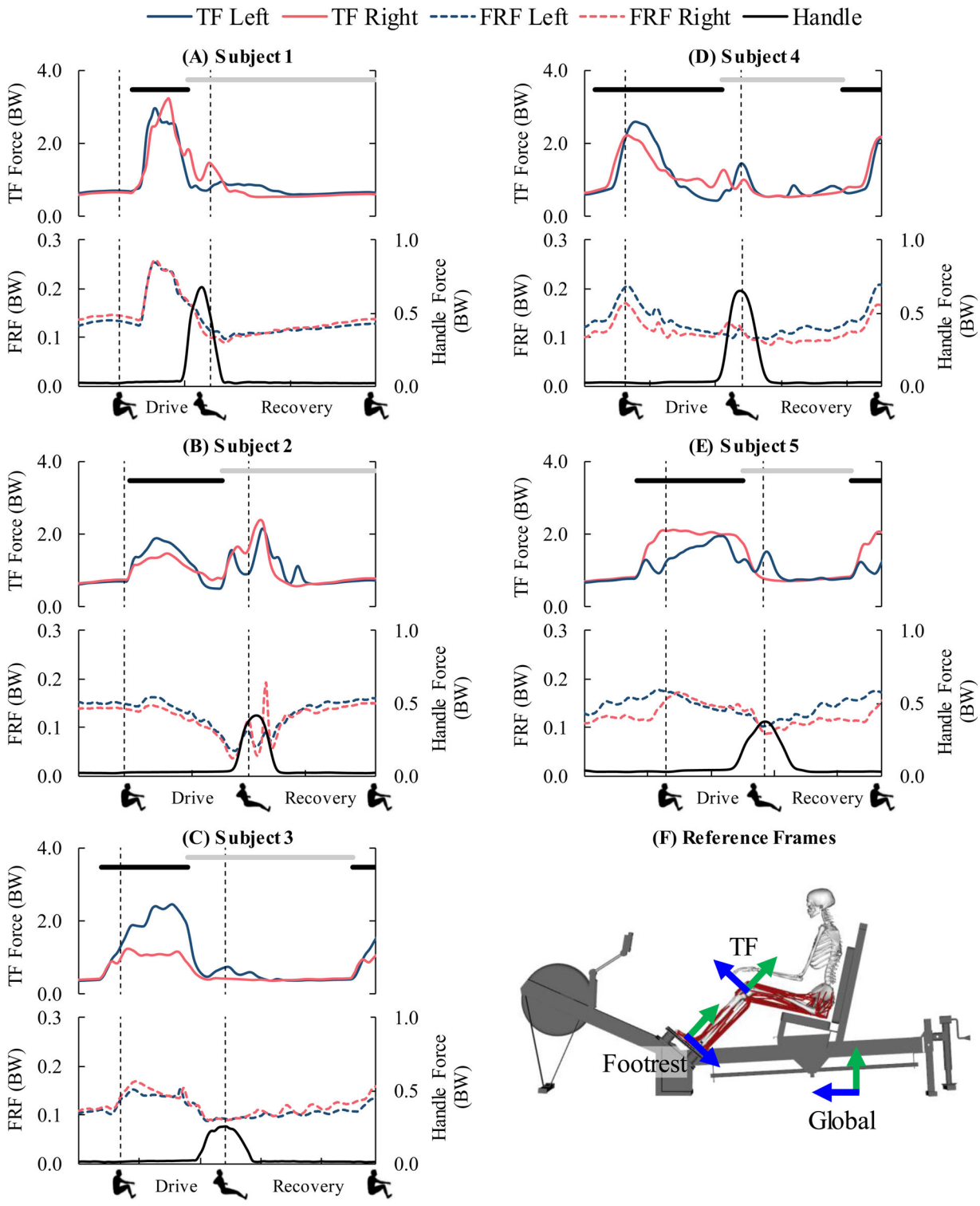

Figure 6. Magnitudes of tibiofemoral (TF), foot reaction, and handle forces during FES rowing from five individuals with SCI (A-E), and reference frames for reporting the forces (F). The TF forces were represented in the leg-specific TF reference frames. The foot reaction forces (FRFs) were represented in the leg-specific footrest reference frames. The handle forces were represented in the global reference frame. The first dashed vertical line represents the beginning of the drive phase of rowing, while the second vertical line represents the beginning of the recovery phase of rowing. The solid black horizontal lines represent the intervals of stimulation of the quadriceps muscles, and the solid gray lines represent the intervals of stimulation of the hamstrings muscles.

surrogate measure for bone mechanical stimulus at the knee during exercise. Similarly, our results showing significant associations between peak tibiofemoral forces and peak handle forces (Figure 4(C,D))

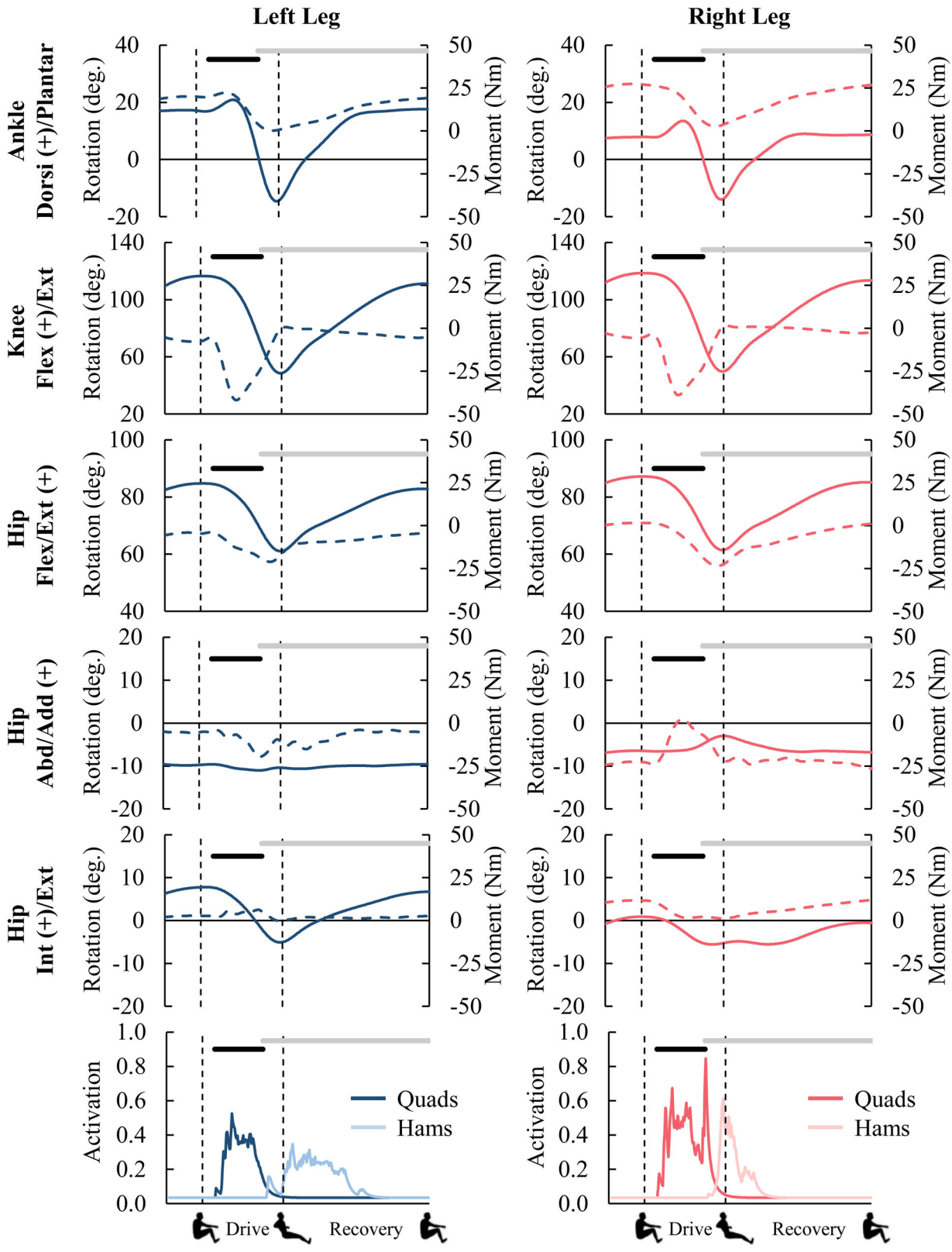

Figure 7. Joint kinematics (solid lines), corresponding joint moments (dashed lines), and CMC-predicted muscle activations from a representative individual with SCI (Subject 1) during FES rowing. Quadriceps muscles activations comprise the magnitude of activations from the rectus femoris, vastus medialis, and vastus lateralis muscles. Hamstrings muscles comprise the magnitude of activations from the semimembranosus, semitendinosus, and biceps femoris long head muscles. The first dashed vertical line represents the beginning of the drive phase of rowing, while the second vertical line represents the beginning of the recovery phase of rowing. The solid black horizontal lines represent the intervals of stimulation of the quadriceps muscles, and the solid gray lines represent the intervals of stimulation of the hamstrings muscles.

suggest that inexpensive force transducers mounted to the handles of exercise machines (when applicable) may provide another surrogate measure for bone mechanical stimulus at the knee.

This study provides quantitative evidence on the differences between measured FRFs and tibiofemoral forces during FES rowing. Previous studies investigating the effects of FES rowing on bone health have speculated on these differences, but supporting evidence has been sparse (Lambach et al. 2020; Draghici et al. 2019). For example, Lambach et al. (Lambach et al. 2020) described that FRFs are not equivalent to forces experienced by the bones. Muscles, ligaments, and other structures within the joints, bone geometry, and the joint angles experienced during FES rowing all contribute to the complex internal forces acting on the bones. They further explained that because FES rowing involves stimulating muscles that span the knee, the forces acting on the distal femur are much higher than the measured FRFs (Lambach et al. 2020). Dragichi et al. corroborated these differences by noting that the distal femur and the proximal tibia may be exposed to even greater loads because of the internal forces from the stimulated muscles crossing the knee joint (Draghici et al. 2019). The results from our study demonstrate that peak magnitudes of tibiofemoral forces are over 10 times greater than peak FRFs, and this ratio is ∼17 times for the compressive components of the forces (Figure 5(A)). Another interesting difference between the measured FRFs and tibiofemoral forces is that the values of peak compressive (0.13–0.14 BW) and AP shear (0.14 BW) FRFs were similar (Figure 3), while the values of compressive tibiofemoral forces (2.19–2.36 BW) were around six times greater than AP shear tibiofemoral forces (0.36–0.42 BW, Figure 2). These differences highlight the importance of incorporating the contributions of muscle forces in quantifying bone mechanical stimulus at the knee during FES rowing.

A limitation of this study is that we did not compute tibiofemoral forces from matched control subjects. Halliday et al. (Halliday et al. 2004) reported substantially greater FRFs and handle forces from five male university varsity-level rowers compared to one male rower with SCI; however, knowledge of tibiofemoral forces from able-bodied rowers remains unknown. A second limitation is that in the musculoskeletal model we used previously-published values of maximum isometric muscle forces obtained from healthy young adults (Rajagopal et al. 2016). We did not acquire joint strength data from our participants with SCI, and we did not scale the maximum isometric muscle force values to reflect the diminished strength of individuals after SCI. This assumption resulted in less than maximal activations of the quadriceps and hamstrings muscles to reproduce the FES rowing motion in our five participants with SCI. A third limitation of this study is that our simplified knee joint did not permit internal-external or abduction-adduction rotations. Allowing these DoFs would require the knee muscles to balance net moments in these directions. We speculate that balancing moments in these additional DoFs would increase the tibiofemoral forces reported in this study. A fourth limitation is our sample size of five participants. A larger study with more participants is required to generalize the findings of this study. A fifth potential limitation is the large RMS errors between the CMC-predicted and inverse dynamics-based knee joint moments (Figure 8). Errors in knee joint moments affect tibiofemoral force predictions. A possible reason for these errors is that we did not measure seat forces during rowing, and these external forces were not included in our simulations. Next, our manual process of adjusting optimal fiber length and tendon slack length of each of the lower extremity muscles is a limitation; objective criteria-based optimization methods are a more rigorous approach for estimating these muscle parameters. Finally, our choice of the computational framework to determine tibiofemoral forces was based on CMC's ability to selectively activate the quadriceps and hamstrings muscle groups, which is necessary to simulate FES rowing. There are other computational methods (such as static optimization, direct colocation, and optimal control) that may be able to simulate FES rowing; the utility of these methods to determine tibiofemoral forces during FES rowing is yet to be determined.

This study addresses a critical roadblock in developing a direct exercise intensity metric for bone mechanical stimulus at the knee, the most common site for fragility fractures after SCI. An adequate mechanical stimulus is necessary to maintain bone health since bone loss after SCI is in large part due to disuse. Currently, clinicians prescribe exercises to SCI patients to provide mechanical stimulus to the bones at the knee, but there is no direct method to quantify the bone mechanical stimulus at the knee. A direct metric for bone mechanical stimulus at the knee requires knowledge of the tibiofemoral forces during exercise. Our work demonstrates a computational approach to quantify tibiofemoral forces during FES rowing. This ability to compute tibiofemoral joint forces during exercise, along with the number of

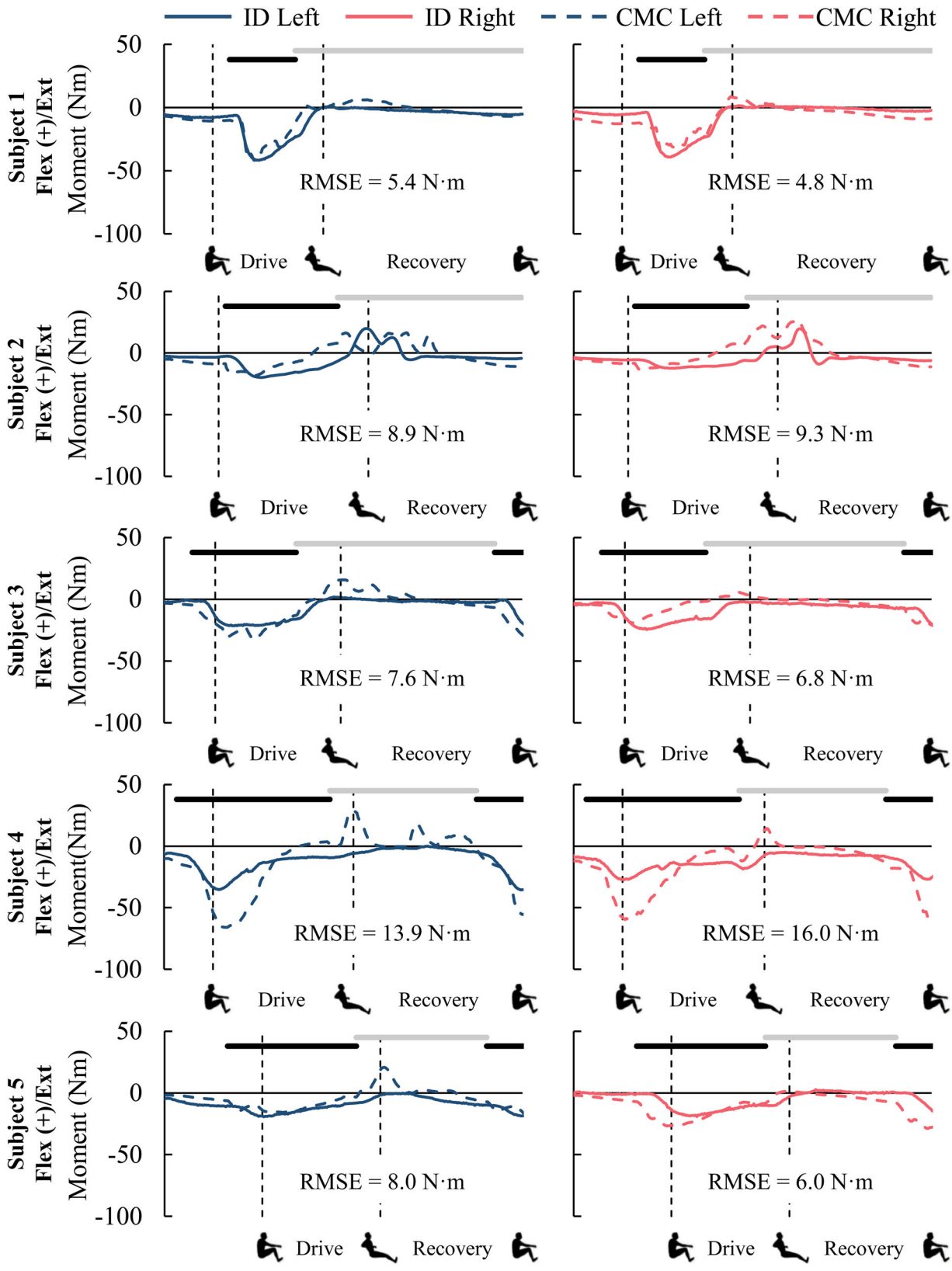

Figure 8. Knee joint moments from inverse dynamics (ID) and Computed Muscle Control (CMC) during FES rowing from all five participants. The root mean square errors (RMSE) between the ID and CMC-predicted moments are included for each simulation. The first dashed vertical line represents the beginning of the drive phase of rowing, while the second vertical line represents the beginning of the recovery phase of rowing. The solid black horizontal lines represent the intervals of stimulation of the quadriceps muscles, and the solid gray lines represent the intervals of stimulation of the hamstrings muscles.

loading cycles and frequency of exercise, will provide clinicians an accurate measure of bone mechanical stimulus during an exercise session. In addition, these tibiofemoral forces will provide the necessary boundary conditions to measure bone strain/strain energy, which is considered the primary mechanical driver of bone remodelling (Martelli et al. 2020). The computational framework presented here lays a foundation for optimizing physical rehabilitation after SCI using musculoskeletal modelling to target musculoskeletal tissue mechanobiology (Pizzolato et al. 2019). These advances in technology have the potential to transform physical rehabilitation for bone loss after SCI from current trial-and-error methods to an evidence-based, personalized approach.

Disclosure statement

The authors have no conflict of interest to disclose related to this manuscript.

Funding

This work was supported in part by the United States Department of Veterans Affairs, Rehabilitation Research and Development Service (grant number I21 RX001410).

ORCID

Gary S. Beaupre http://orcid.org/0000-0002-6211-7621

References

Alekna V, Tamulaitiene M, Sinevicius T, Juocevicius A. 2008. Effect of weight-bearing activities on bone mineral density in spinal cord injured patients during the period of the first two years. Spinal Cord. 46(11):727–732.

Andrews B, Gibbons R, Wheeler G. 2017. Development of functional electrical stimulation rowing: the Rowstim series. Artif Organs. 41(11):E203–E212.

Bauman WA, Cardozo CP. 2015. Osteoporosis in individuals with spinal cord injury. PM R. 7(2):188–201. quiz 201.

Beck BR, Snow CM. 2003. Bone health across the lifespan-exercising our options. Exerc Sport Sci Rev. 31(3): 117–122.

Ben M, Harvey L, Denis S, Glinsky J, Goehl G, Chee S, Herbert RD. 2005. Does 12 weeks of regular standing prevent loss of ankle mobility and bone mineral density in people with recent spinal cord injuries? Aust J Physiother. 51(4):251–256.

Bloomfield SA, Mysiw WJ, Jackson RD. 1996. Bone mass and endocrine adaptations to training in spinal cord injured individuals. Bone. 19(1):61–68.

Chen SC, Lai CH, Chan WP, Huang MH, Tsai HW, Chen JJ. 2005. Increases in bone mineral density after functional electrical stimulation cycling exercises in spinal cord injured patients. Disabil Rehabil. 27(22): 1337–1341.

Clark JM, Jelbart M, Rischbieth H, Strayer J, Chatterton B, Schultz C, Marshall R. 2007. Physiological effects of lower extremity functional electrical stimulation in early spinal cord injury: lack of efficacy to prevent bone loss. Spinal Cord. 45(1):78–85.

Deley G, Denuziller J, Casillas JM, Babault N. 2017. One year of training with FES has impressive beneficial effects in a 36-year-old woman with spinal cord injury. J Spinal Cord Med. 40(1):107–112.

Delp SL, Anderson FC, Arnold AS, Loan P, Habib A, John CT, Guendelman E, Thelen DG. 2007. OpenSim: open-source software to create and analyze dynamic simulations of movement. IEEE Trans Biomed Eng. 54(11): 1940–1950.

Delp SL, Loan JP, Hoy MG, Zajac FE, Topp EL, Rosen JM. 1990. An interactive graphics-based model of the lower extremity to study orthopaedic surgical procedures. IEEE Trans Biomed Eng. 37(8):757–767.

DeMers MS, Pal S, Delp SL. 2014. Changes in tibiofemoral forces due to variations in muscle activity during walking. J Orthop Res. 32(6):769–776.

Dolbow DR, Gorgey AS, Dolbow JD, Gater DR. 2013. Seat pressure changes after eight weeks of functional electrical stimulation cycling: a pilot study. Top Spinal Cord Inj Rehabil. 19(3):222–228.

Dolbow DR, Gorgey AS, Khalil RK, Gater DR. 2017. Effects of a fifty-six month electrical stimulation cycling program after tetraplegia: case report. J Spinal Cord Med. 40(4):485–4884.

Draghici AE, Taylor JA, Bouxsein ML, Shefelbine SJ. 2019. Effects of FES-rowing exercise on the time-dependent changes in bone microarchitecture after spinal cord injury: a cross-sectional investigation. JBMR Plus. 3(9): e10200.

Eser P, Frotzler A, Zehnder Y, Denoth J. 2005. Fracture threshold in the femur and tibia of people with spinal cord injury as determined by peripheral quantitative computed tomography. Arch Phys Med Rehabil. 86(3): 498–504.

Eser P, Frotzler A, Zehnder Y, Wick L, Knecht H, Denoth J, Schiessl H. 2004. Relationship between the duration of paralysis and bone structure: a pQCT study of spinal cord injured individuals. Bone. 34(5):869–880.

Fornusek C, Davis GM, Russold MF. 2013. Pilot study of the effect of low-cadence functional electrical stimulation cycling after spinal cord injury on thigh girth and strength. Arch Phys Med Rehabil. 94(5):990–993.

Frotzler A, Coupaud S, Perret C, Kakebeeke TH, Hunt KJ, Donaldson N. d N, Eser P. 2008. High-volume FES-cycling partially reverses bone loss in people with chronic spinal cord injury. Bone. 43(1):169–176.

Giangregorio LM, Hicks AL, Webber CE, Phillips SM, Craven BC, Bugaresti JM, McCartney N. 2005. Body weight supported treadmill training in acute spinal cord injury: impact on muscle and bone. Spinal Cord. 43(11): 649–657.

Gibbons RS. 2015. FES-rowing in tetraplegia: the effect of functional electrical stimulation-assisted rowing on cardiac structure and function and bone mineral density in

persons with spinal cord injury [PhD dissertation]. London: Brunel University.

Gibbons RS, Beaupre GS, Kazakia GJ. 2016. FES-rowing attenuates bone loss following spinal cord injury as assessed by HR-pQCT. Spinal Cord Ser Cases. 2:15041.

Gibbons RS, McCarthy ID, Gall A, Stock CG, Shippen J, Andrews BJ. 2014. Can FES-rowing mediate bone mineral density in SCI: a pilot study. Spinal Cord. 52(S3): S4–S5.

Goemaere S, Van Laere M, De Neve P, Kaufman JM. 1994. Bone mineral status in paraplegic patients who do or do not perform standing. Osteoporosis Int. 4(3):138–143.

Gorgey AS, Lawrence J. 2016. Acute responses of functional electrical stimulation cycling on the ventilation-to-CO2 production ratio and substrate utilization after spinal cord injury. PM R. 8(3):225–234.

Grassner L, Klein B, Maier D, Buhren V, Vogel M. 2018. Lower extremity fractures in patients with spinal cord injury Characteristics, outcome and risk factors for non-unions. J Spinal Cord Med. 41(6):676–683.

Griffin L, Decker MJ, Hwang JY, Wang B, Kitchen K, Ding Z, Ivy JL. 2009. Functional electrical stimulation cycling improves body composition, metabolic and neural factors in persons with spinal cord injury. J Electromyogr Kinesiol. 19(4):614–622.

Halliday SE, Zavatsky AB, Hase K. 2004. Can functional electric stimulation-assisted rowing reproduce a race-winning rowing stroke? Arch Phys Med Rehabil. 85(8): 1265–1272.

Johnston TE, Marino RJ, Oleson CV, Schmidt-Read M, Leiby BE, Sendecki J, Singh H, Modlesky CM. 2016. Musculoskeletal effects of 2 functional electrical stimulation cycling paradigms conducted at different cadences for people with spinal cord injury: a pilot study. Arch Phys Med Rehabil. 97(9):1413–1422.

Krause JS, Carter RE, Pickelsimer EE, Wilson D. 2008. A prospective study of health and risk of mortality after spinal cord injury. Arch Phys Med Rehabil. 89(8): 1482–1491.

Lambach RL, Stafford NE, Kolesar JA, Kiratli BJ, Creasey GH, Gibbons RS, Andrews BJ, Beaupre GS. 2020. Bone changes in the lower limbs from participation in an FES rowing exercise program implemented within two years after traumatic spinal cord injury. J Spinal Cord Med. 43(3):306–314.

Martelli S, Beck B, Saxby D, Lloyd D, Pivonka P, Taylor M. 2020. Modelling human locomotion to inform exercise prescription for osteoporosis. Curr Osteoporos Rep. 18(3):301–311.

Mohr T, Pødenphant J, Biering–Sørensen F, Galbo H, Thamsborg G, Kjaer M. 1997. Increased bone mineral density after prolonged electrically induced cycle training of paralyzed limbs in spinal cord injured man. Calcif Tissue Int. 61(1):22–25.

Morse LR, Battaglino RA, Stolzmann KL, Hallett LD, Waddimba A, Gagnon D, Lazzari AA, Garshick E. 2009a. Osteoporotic fractures and hospitalization risk in chronic spinal cord injury. Osteoporos Int. 20(3):385–392.

Morse LR, Geller A, Battaglino RA, Stolzmann KL, Matthess K, Lazzari AA, Garshick E. 2009b. Barriers to providing dual energy x-ray absorptiometry services to individuals with spinal cord injury. Am J Phys Med Rehabil. 88(1):57–60.

Nichols JF, Palmer JE, Levy SS. 2003. Low bone mineral density in highly trained male master cyclists. Osteoporos Int. 14:644–649.

Pacy PJ, Hesp R, Halliday DA, Katz D, Cameron G, Reeve J. 1988. Muscle and bone in paraplegic patients, and the effect of functional electrical stimulation. Clin Sci. 75(5): 481–487.

Pizzolato C, Saxby DJ, Palipana D, Diamond LE, Barrett RS, Teng YD, Lloyd DG. 2019. Neuromusculoskeletal modeling-based prostheses for recovery after spinal cord injury. Front Neurorobot. 13:97.

Rajagopal A, Dembia CL, DeMers MS, Delp DD, Hicks JL, Delp SL. 2016. Full-body musculoskeletal model for muscle-driven simulation of human gait. IEEE Trans Biomed Eng. 63(10):2068–2079.

Shields RK, Dudley-Javoroski S. 2007. Musculoskeletal adaptations in chronic spinal cord injury: effects of long-term soleus electrical stimulation training. Neurorehabil Neural Repair. 21(2):169–179.

Steele KM, Demers MS, Schwartz MH, Delp SL. 2012. Compressive tibiofemoral force during crouch gait. Gait Posture. 35(4):556–560.

Szollar SM, Martin EM, Sartoris DJ, Parthemore JG, Deftos LJ. 1998. Bone mineral density and indexes of bone metabolism in spinal cord injury. Am J Phys Med Rehabil. 77(1):28–35.

Thelen DG, Anderson FC, Delp SL. 2003. Generating dynamic simulations of movement using computed muscle control. J Biomech. 36(3):321–328.